"COMPUTATIONAL ANALYSIS OF HEAT TRANSFER THROUGH RECTANGULAR CHANNEL USING BOOT SHAPE RIB TURBULATORS"

Kyada Hiten[1*], Lakkad Harsh[1], Dave Rutvik[2], Asmaniwala Harsh[2], Dr. K Vijayaraja[3]

[1]B.E.(Department of Aeronautical engineering) Student, KCG College of Technology, Chennai, Tamilnadu, India
[2]B.E.(MED)Student, Shree Swami Atmanand Saraswati Institute of Technology, Surat, Gujarat, India
[3]Head of Department(Aeronautical engineering) , KCG College of Technology, Chennai, Tamilnadu, India
*Author of Correspondence E-mail: hitenkyada12@gmail.com

---***---

Abstract - This work deals with the computational analysis of the boot shaped ribs of different cross-section. Computational domain of 100mmx100mmx300mm has been created using CATIA and then analyzed using Ansys. The boot shaped rib of 3mm,6mm,9mm,12mm height are analyzed with operational conditions of Reynolds numbers 10000,20000,30000,40000,50000 and 60000. the copper material is used for ribs and the fluid used here is air. the essential parameters such as heat transfer rate, friction factor, wall shear stress, turbulence kinetic energy, pressure difference and temperature distribution, Nusselt number, enthalpy variation of both working fluid and heating surface are analyzed. Its observed from computational results that the increase in rib height and Reynolds number will create more turbulence.

*Key Words***:** Heat Transfer, Turbulence, Ribs, Rynolds number, Nusselt number, Channel

1.INTRODUCTION

Gas turbines play a vital role in today's world and as the demand for power increases, the thermal efficiency and power output of the engine should be optimized. Gas turbines are the most sophisticated mechanical machines as per power generation is concerned in Aircraft Jet Engines and also in power plants. One method of increasing both the power output and thermal efficiency is to increase the inlet temperature of the hot gases through the internal passages. The efficiency of jet engines is enhanced by increasing the combustion temperature which enables the turbine to run with higher rpm. But this increase in temperature may lead to melting of turbine blades which is a major cause for turbine blades failure. The gas turbine is a rotary engine that extracts power from the flow of combustion gases. Energy is extracted in the form of shaft power and thrust. The gas turbines are described thermodynamically by the Brayton cycle, in which air is compressed isentropically, combustion occurs at constant pressure and expansion over the turbine occurs isentropically back to the starting pressure. In advanced gas turbines, the turbine inlet temperature of the gases is as high as 1700° C – 2000° C. These temperatures exceed the melting point of the turbine components. Therefore, it is very important to cool the turbine components so that they can withstand these extreme temperatures. With current cooling techniques, the temperature is decreased to almost 1000° C so that they can withstand this extreme environment.

Mi-Ae Moon [1]. Effects of blade rotation are reduced by the ribs and heat transfer is not different for both walls in the second pass. Also, the rotational effects are identical for both blockage ratios. From the correlations heat transfer in the extended range is predicted by the buoyancy parameter. Michael Huh et al. [2]. Using liquid crystal thermography, the depiction of the local heat transfer coefficient in the inter-rib regions has been reconstructed. The average Nusselt number and by the friction factor depicted thermal performance of each ribbed channel. Improved heat transfer performances were observed at the optimal rib with the pitch-to-height ratio of 13.33 for the one-ribbed wall channel and at p/e = 6.66–10 for the two-ribbed wall channel.

Giovanni Tanda et al. [3]. The internal flow pattern and heat transfer characteristics in the channel with air-only are conducted at two kinds of temperature difference. The results indicate that the 39 K temperature difference provides a slightly better heat transfer performance than that of the 60 K temperature difference. In addition, the obtained results show that the mist/steam gives the best heat transfer enhancement and thermal performance in the channel. The detailed flow pattern and Nusselt number distribution for four coolants are also illustrated and discussed. Feng Zhang et al. [4]. The cooling effect of the test vane with newly designed cooling structure is high (approximately 0.8) and uniformly distributed. The entropy creation of external air cooling due to external mixing is higher than the heat transfer, and for the steam convective cooling, the entropy creation due to internal friction is much higher than heat transfer in the cooling process.

Wang et al. [5]. Detailed discussion on rib induced secondary flows and rotational effects on heat transfer in smooth and rib roughened duct are presented in this paper using results obtained from detailed heat transfer measurements from experiments and fluid dynamics predictions from numerical simulations. Prashant Singh et al. [6]. The heat transfer enhancement capability of each channel configuration is evaluated and comparisons of infrared results and numerical predictions are made. Finally, the channel overall heat transfer coefficient and friction ratio are evaluated on each configuration. Summarizing the results, it can be estimated that, the cooling performance inside trailing edge internal cooling passages can be elevated by arranging dimples and protrusions,

or the combination with other typical devices such as ribs or pin–fins. Zhong yang Shen et al. [7]. As compared to the smooth duct, the turbulator roughened duct enhances the heat transfer and friction factor by 2.82 and 3.72 times, respectively. The correlations have been developed for area averaged Nusselt number and friction factor for turbulator roughened duct. Santosh B.

Bopche. et al [8]. Study on various offset mid-truncated ribs aiming to improve the heat transfer of turbine blade internal cooling passages with reduced pressure loss penalty. Gongnan Xie. et al. [9]. The cross-flow does not show detrimental effects on the heat transfer of the downstream inlet jets in the swirl tube S5. In support of the experiments, three-dimensional numerical computations are presented to provide more insight into the flow structure in the swirl tubes. et al. [10]. The overall thermal performance is greatly improved by the internal-protruded dimples compared with the conventional spherical dimples without the addition of added heated surface areas. et al. [11]. The end walls Nusselt numbers (Nu) distributions, Fanning friction factors(f) and thermal performance factors (TPF) for a stationary S-shaped two-pass square channel with the associated turbulent flow fields analyzed by ANSYS Fluent code Pey-Shey Wu. [12]. The use of dimples is suitable for augmenting blade tip cooling to achieve an optimal balance between thermal and mechanical design requirements. Gongnan Xie. et al. [13].

Nomenclature:

Re	Reynold's Number
T	Wall Shear stress(N/m^2)
h	Specific Enthalpy (J/kg)
Nu	Nusselt Number
K	Turbulent kinetic energy(kg-m^2/s^2)
p	Effective Pressure (Pa)
T	Temperature(K)
C_f	Skin friction coefficient
Df	Specific Heat (J/kg-K)
ρ	Density(kg/m3)
μ	Dynamic Viscosity (kg/ms)
α	Thermal diffusivity (m^2/s)
ϵ	Strain
k	Thermal conductivity (W/m-k)
u_i,u_j	Initial velocities in i&j direction(m/s)
u_i,u_j	Final velocities in i&j direction (m/s)

Gongnan Xie. et al. [13].The high rpm reduces the heat transfer coefficient on the rotor due to the low rotor relative velocity and increases the ''sweet spot" on the rotor tip. Huitao Yang et al. [14]. ribbed-to-smooth thermal performance is significantly elevated by rotation when the rotation number reaches over 0.25. Hongwu Deng et al. [15]. The Pareto-optimal solutions of the fan-shaped pin–fin show that the designs were improved with respect to heat transfer and pressure drop in comparison with the circular and reference pin–fins. MI-Ae Moon et al. [16]. The heat/mass transfer performance was significantly enhanced for all channel aspect ratios when an intersecting rib was added to an ordinary angled rib configuration. Heeyoon Chung et al [17]. Flow inside ducts, the mass-flow-averaged temperature (T_m) and the adiabatic wall temperature (T_{aw}) are often used as a mainstream reference temperature. To resolve the mainstream reference temperature from the measured temperatures at several locations using non-dimensional temperature analysis. R. Kan et al [18]. The thermal performance of dimpled channel with bleed hole is comparable to typical rib and pin–fin channel. Better performance on friction ratio and thermal performance will be obtained after the bleed extraction effect.

Zhong yang Shen et al [19] In this report, with the references of the above literature survey, the effects of boot shaped ribs with different heights at different Reynolds number in heat transfer have been discussed. In this work boot shaped ribs with four different heights (3mm, 6mm, 9mm, and 12mm) have been used for computational work. And CFD simulation methodology has been adopted for analyzing and comparison of the heat transfer rate for various boot shaped ribs with different heights at different Reynolds Number (Re. 10000, 20000, 30000, 40000, 50000, and 60000).
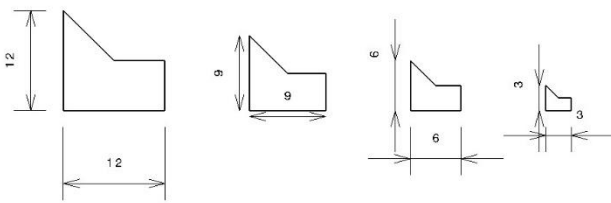
In this paper, with the references of the above literature survey, the effects of boot-shaped ribs with different heights at different Reynolds number in heat transfer have been discussed. In this work boot shaped ribs with four different heights (3mm, 6mm, 9mm, and 12mm) have been used for computational work. And CFD simulation methodology has been adopted for analyzing and the comparison is made for heat transfer rate for various boot shaped ribs with different heights at different Reynolds Number (Re. 10000, 20000, 30000, 40000, 50000, and 60000). Computational results have been validated by results obtained by experiment.

2. Model description

The model uses a test section of the turbine blade of length 300mm. The cross-sectional area of the test section is 100*100 mm2and it is constant throughout the section. The aspect ratio of the rib is taken as 1(AR =W/H). The cross-section of the boot-shaped ribs of height (H) and width (W) of 3mm, 6mm and 9mm, 12mm and without ribs are shown in figure.1. Plain channel, channel with Rectangular cross-section is chosen and boot-shaped ribs of different heights i.e. 3mm, 6mm, 9mm and 12mmare shown in the following figure.1.

All dimensions are in mm

Figure.1. Cross-sectional 2D View of sharp boot rib with various dimensions

(a) Plain channel

(b) Channel with 3mm ribs

(c) Channel with 6mm ribs

(d) Channel with 9mm ribs
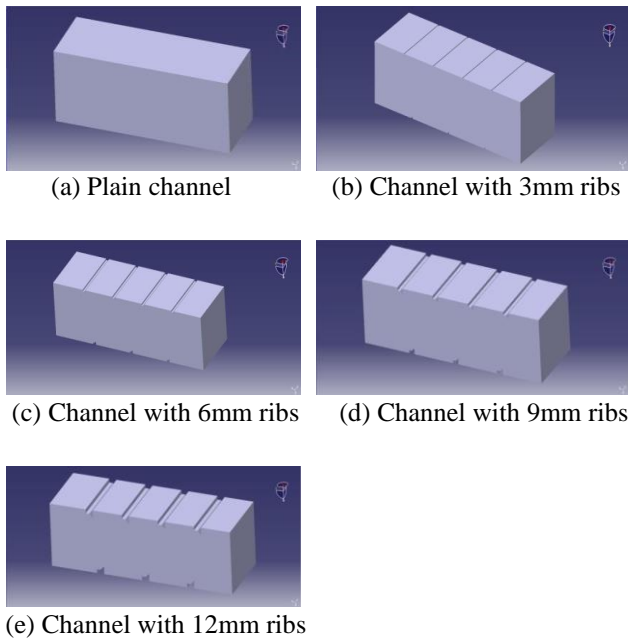
(e) Channel with 12mm ribs

Figure 2. Modeling of Rectangular channel with various dimensions of ribs

2.1 Meshing

In order to do the experimental analysis, the model shown in the figures above is imported in the ANSYS Workbench 13.0 Fluid Flow (Fluent). Meshing is done with fine relevance center and high smoothing. The maximum face size and maximum size are given as 1.40 mm. The mesh generated in this model is as followed in figure.3.

(a) Plain

(b) 3mm Boot shape Ribs

(c) 6mm Boot Shape Ribs

(d) 9mm Boot Shape Ribs

(e) 12mm Boot Shape Ribs
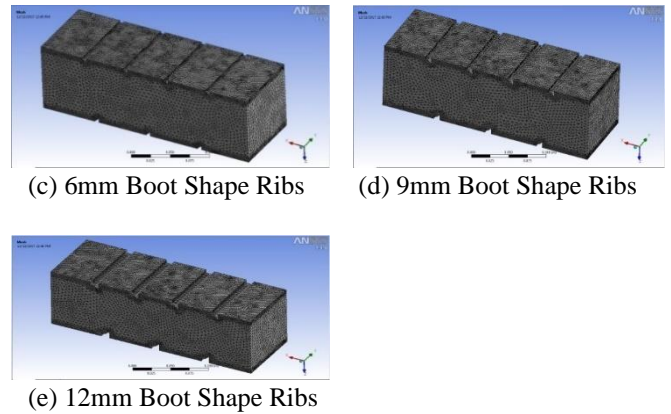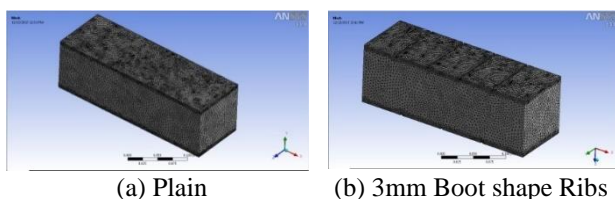
Figure 3. Meshing of Rectangular channel with various dimension of ribs

3. Numerical Method

The turbulent flow fields in the S-shaped two-pass square channel of the present study are analyzed by ANSYS Fluent code to disclose the flow structures responsive to the measured thermal performances. The computational domain is chosen to be the flow regions shown in Continuity, momentum, energy, and turbulence equations are solved iteratively with SIMPLE algorism. Uniform velocity corresponding to desired Reynolds number is specified at the inlet to the inlet leg, while a pressure outlet condition is applied at the exit of the outlet leg. The specification of pressure outlet condition gives better convergence and accuracy than the outflow boundary condition for the flow may have recirculation, or velocity gradients may not be negligible, at the exit due to the vortices shed from the sharp turn and the two undulant edges of the S-shaped channel. Uniform heat flux with the same value as deduced from experiments is applied to the heated wall. The computed exit bulk temperature must agree with the measured value to within 0.2 C to ensure energy balance. As the uniform heat flux heating conditions are imposed over the two opposite heating foils, the streamwise T_b variations are assumed to increase linearly along the test channel. Using the measured T_b data at the flow entry and exit to define the slope of the streamwise T_b increase along the test channel, local T_b values are accordingly determined for calculating local Nu based on the local T_w generated by the CFD code. Residuals for the convergence of iterations are set to 1E-6 for energy equation and 1E-4 for all other equations. From the converged solutions of various turbulence models, including k-e family (Standard, RNG, and Realizable k-e models) and Reynolds Stress Model (RSM), the computed overall averaged Nu is compared with the measured data at Re = 15,000. Deviation in the range of 14.4 to 34.3% was obtained. It was found that RNG k-e model gave the best agreement with the measured heat transfer results while RSM had the worst deviation.

The computational domain is meshed with tetrahedral elements. Green-Gauss node based spatial discretization scheme was chosen in the solution heated wall is also indicated. For these fine grids used in this study, enhanced wall treatment (EWT) which combines two-layer enhanced wall functions is

used to account for the viscosity-affected near-wall region and resolve the turbulence behavior all the way down to viscous sublayer. The Nu results have an insignificant difference for the number of elements ranging from 1.8 to 3.5 million. However, when the number of elements reaches 3.5 million, the required CPU time becomes unpractical.

The computed overall averaged Nu at different Re using RNG k-e model are compared with experimental data, as shown. The absolute values of deviations compared to the measurements vary from 6.5% (at Re = 5000) to 14.4% (at Re = 15,000). Results of Standard k-e model having absolute deviation range of 10.8% (at Re = 5000)–18.4% (at Re = 15,000) are also shown. From the theoretical foundation of the models, the improvement of RNG k-e model over Standard k-e model is believed to be mainly due to improved e equation for rapidly strained flows and inclusion of swirling effect and analytically calculated turbulent Prandtl numbers. Both the experimentally methods. A body-size control parameter was used to limit the largest element size. Ten prism layers with a growth rate of 1.2 and the transition ratio of 0.272 were generated normal to the heated wall to resolve strong temperature and velocity gradients near the wall. A grid independence test using RNG k-e model with averaged Nu of the inlet leg as the examined quantity is shown.

3.1 Normalizing Nusselt Number

A Nusselt number is a dimensionless number which is used to estimate the heat transfer component. It is the ratio of convective to conductive heat transfer coefficients across the boundary. The Nusselt number, Nu no. is given by equation (1).

$$Nu = {hD}/{k} \qquad (1)$$

where, h= heat transfer coefficient, W/m^2K D = characteristic length, m k = thermal conductivity of the fluid, W/ K

The value of characteristic length depends on the type of the channel. The value of thermal conductivity of the fluid, air in our case is 0.025 W/m K.

The local heat transfer coefficient is calculated from the local net heat transfer rate per unit surface area from wall to cooling air; local wall temperature and local bulk mean temperature.

$$h = \frac{({q}/{A})}{(T_w - T_b)} \qquad (2)$$

where,

q/A = heat transfer per unit area, W/m^2
T_w = local wall temperature, K
T_b = local bulk mean air temperature, K

The bulk means temperature entering and leaving the section is obtained. The local bulk mean temperature, T_b is calculated by assuming a linear rise along the stream-wise flow. The local wall temperature, T_w is also obtained. From these results, the heat transfer coefficient is calculated by applying it in equation (2).

The Nusselt number is calculated by applying the heat transfer coefficient values in equation (1). The obtained Nusselt number is now averaged. The normalizing factor is provided by the correlation by Dittus – Boelter equation for Nusselt number for fully developed turbulent flow for smooth tubes provided in equation (3).

$$Nu_{FD} = 0.023 \, Re^{0.8} Pr^n \qquad (3)$$

where,

Nu_{FD} = Nusselt number for fully developed turbulent flow
Re = Reynolds number Pr = Prandtl number n = constant.
The value for n = 0.4 for smooth tubes.

The Dittus – Boelter equation is an explicit function to calculate the Nusselt number. It is easy to solve and is completely tailored for the smooth channels.

The normalized Nusselt number is obtained by dividing the Nusselt number and the normalizing factor.

$$Nu_{norm.} = {Nu}/{Nu_{FD}} \qquad (4)$$

3.2 Boundary Conditions

The boundary conditions are assigned and the model is meshed in Setup and Solution window. The experiments are done for Reynolds number of 10000, 20000, 30000, 40000, 50000 and 60000; the solver type is assigned as Pressure based, with absolute velocity formulation and steady time. The energy equation is switched ON and the viscous model is chosen as 'RNG k-epsilon'. The air is sent to the inlet as a coolant. The thermal condition in the copper wall is chosen as heat flux and the value is assigned as 4000 W/m^2 which is common for both the top and bottom walls. The side walls are assumed to be adiabatic. The boundary condition at the inlet is given as the velocity magnitude of 1.461m/s, 2.921m/s, 4.382m/s, 5.843m/s, 7.303m/s and 8.764m/s which are based on Reynolds number of 10000, 20000, 30000, 40000, 50000 and 60000 for the models. The reference value is assigned, to be computed from 'inlet' and the reference zone is selected as 'solid'. The residual monitor values are assigned as 0.0001 for all residuals along x, y and z directions and also for continuity equation. It is assigned as 1e-6 for energy equation and 0.0001 for k and epsilon. The initialization is assigned as standard and is made to compute from the inlet.

3.3 Governing Equation

The analysis has been carried out in ANSYS Fluent software it is based on Finite Volume Method to solve the Navier Stokes Equation and energy equations The governing equations of continuity, momentum and energy equations for the steady-state incompressible flow with the steady state, incompressible flow with constant physical properties are shown in Equations (1), (2) and (3) respectively. The RNG K-epsilon Turbulence equation is derived in equations (4) and (5). The effects of natural convection and radiation are negligible.

$$\frac{\partial u_i}{\partial x_i} = 0 \quad (1)$$

$$\frac{\partial}{\partial x_j}(\rho u_i u_j) = -\frac{\partial P}{\partial x_i} + \frac{\partial}{\partial x_j}\left[\mu\left(\frac{\partial u_i}{\partial x_j} + \frac{\partial u_j}{\partial x_i} - \frac{2}{3}\delta_{ij}\frac{\partial u_l}{\partial x_l}\right)\right] + \frac{\partial}{\partial x_j}(-\rho u_i' u_j') \quad (2)$$

$$\frac{\partial}{\partial x_i}\left(u_i(\rho\epsilon + p)\right) = \frac{\partial}{\partial x_i}\left(k_{eff}\frac{\partial T}{\partial x_j}\right) \quad (3)$$

$$\frac{\partial}{\partial t}(\rho k) + \frac{\partial}{\partial x_i}(\rho k u_i) = \frac{\partial}{\partial x_i}\left(\alpha_k \mu_{eff}\frac{\partial k}{\partial x_j}\right) + G_k + G_b - \rho\epsilon - Y_m + S_k \quad (4)$$

$$\frac{\partial}{\partial t}(\rho\epsilon) + \frac{\partial}{\partial x_i} = \frac{\partial}{\partial x_j}\left(\alpha_\epsilon \mu_{eff}\frac{\partial \epsilon}{\partial x_j}\right) + C_{1\epsilon}\frac{\epsilon}{k}(G_k + C_{3\epsilon}G_b) + C_{1\epsilon}\frac{\epsilon}{k}(G_k + C_{3\epsilon}G_b) - C_{2\epsilon}\rho\frac{\epsilon^2}{k} - R_\epsilon + S_\epsilon \quad (5)$$

3.3 Rib Turbulators

The purpose of introducing the ribs at regular intervals is to enhance the heat transfer rates. Ribs are manmade protrusions which are placed in a controlled way along the walls. The rib induces a separation in the flow and hence causes an increase in the frictional loss. The enhancement of the heat transfer has thus a drawback in the increased pressure drop, which sometimes can be several times larger than for a smooth channel. The pressure drop and heat transfer are strongly connected to the height of the rib. Though the ribs can be placed at a different orientation, our study focuses on the ribs placed orthogonally (at 90 degrees) to the mainstream flow. The size of the rib and the distance between the two successive ribs, the pitch has great importance.

The heat transfer performance of the ribbed channel depends on the channel aspect ratio, rib configuration and Reynolds number of the coolant. When the coolant passes over the ribs, the flow separates and re-attaches as shown in Figure.

Turbulence at different height ribs:

At 3mm height:

Turbulence from velocity vector for 3mm height of the Boot Shaped Ribs at various Reynolds number i.e. at10,000 (fig.4.a), at 20,000 (fig.4.b), at 30,000 (fig.4.c), at 40,000 (fig.4.d), at 50,000 (fig.4.e) and at 60,000 (fig.4.f) have been shown below.

Fig.4.a   Fig.4.b
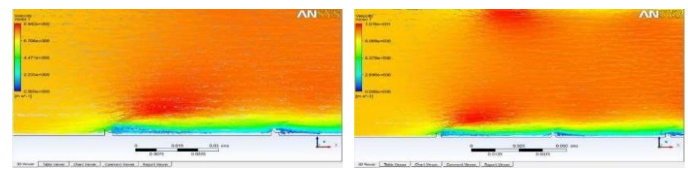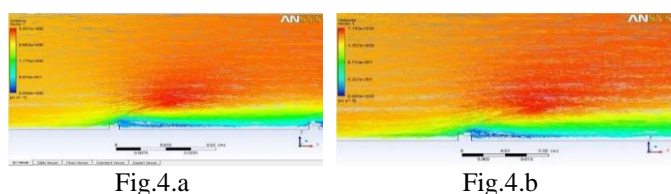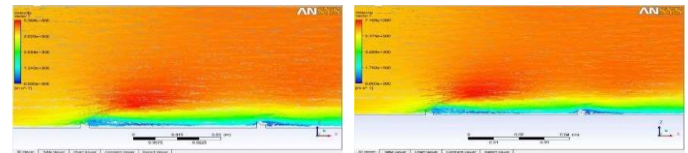

Fig.4.c   Fig.4.d

Fig.4.e   Fig.4.f

At 6 mm height:

Turbulence from velocity vector for 6mm height of the Boot Shaped Ribs at various Reynolds number i.e. at10,000 (fig.5.a), at 20,000 (fig.5.b), at 30,000 (fig.5.c), at 40,000 (fig.5.d), at 50,000 (fig.5.e) and at 60,000 (fig.5.f) have been shown below.
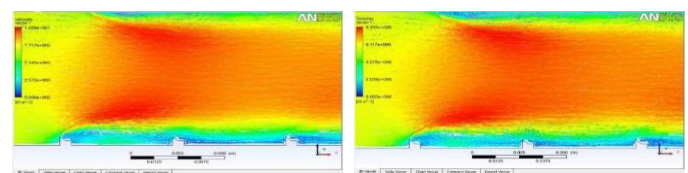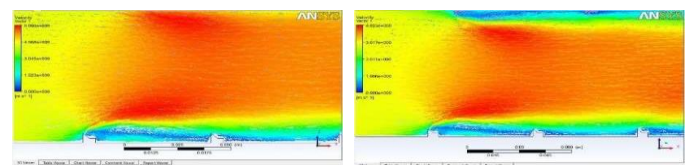

Fig.5.a   Fig.5.b
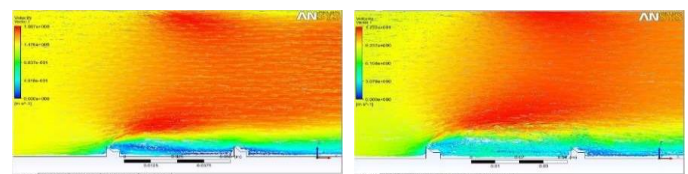

Fig.5.c   Fig.5.d

Fig.5.e   Fig.5.f

At 9 mm height:

Turbulence from velocity vector for 9mm height of the Boot Shaped Ribs at various Reynolds number i.e. at10,000 (fig.6.a), at 20,000 (fig.6.b), at 30,000 (fig.6.c), at 40,000 (fig.6.d), at 50,000 (fig.6.e) and at 60,000 (fig.6.f). have been shown below.
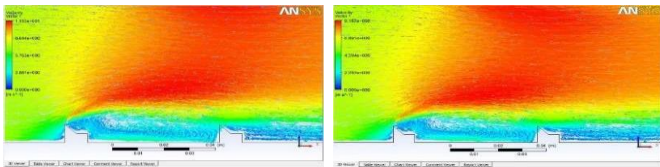
Fig.6.a   Fig.6.b
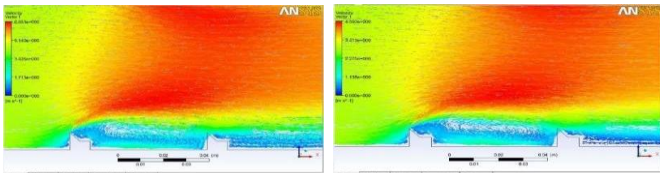

Fig.6.c   Fig.6.d
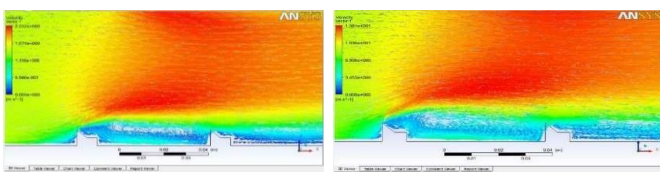

Fig.6.e   Fig.6.f

At 12 mm height:

Turbulence from velocity vector for 12mm height of the Boot Shaped Ribs at various Reynolds number i.e. at 10,000 (fig.7.a), at 20,000 (fig.7.b), at 30,000 (fig.7.c), at 40,000 (fig.7.d), at 50,000 (fig.7.e) and at 60,000 (fig.7.f) have been shown below.
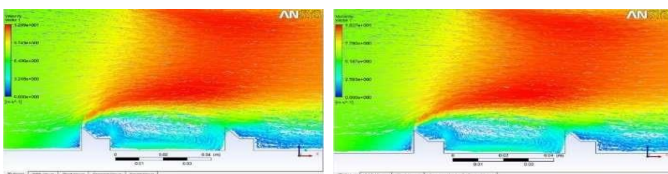

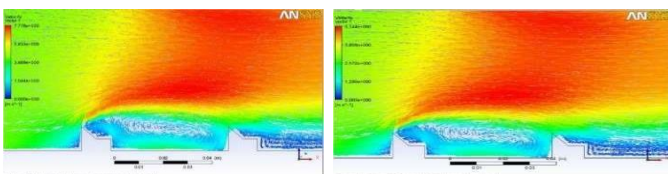
Fig.7.a   Fig.7.b

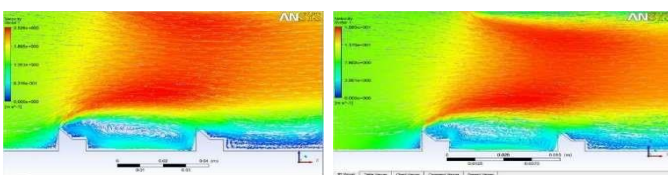Fig.7.c   Fig.7.d

Fig.7.e   Fig.7.f

The velocity vector is the pictorial representation of the flow across the geometry. The turbulence can be easily visualized with the help of the velocity vector. Thus, the velocity vector representation is studied for the different dimensions at various Reynolds number. The representation is given below:

- In the 3mm height of the ribs have the flow of have only happened in the between place of the ribs due to the height is very less
- In 6mm height of the ribs have flow of rotational can happened in the between place of between the turbulators ribs
- In 9mm height of the ribs have the elliptical flow happened in the between place of the ribs but it's happened only the tip portion of the ribs in root position velocity gain is happened
- In 12mm height of the ribs rotational flow happened but the flow in serious first ribs get the rotation second is stable and third rib gets the rotational flows.

4.RESULTS AND DISCUSSION

Following are the lines chosen for representing the different height of the ribs:

3mm   6mm   9mm   12mm   plain channel
─────   ━━━━━   ·······   ▬ ▬ ▬   ─ ─ ─ ─ ─
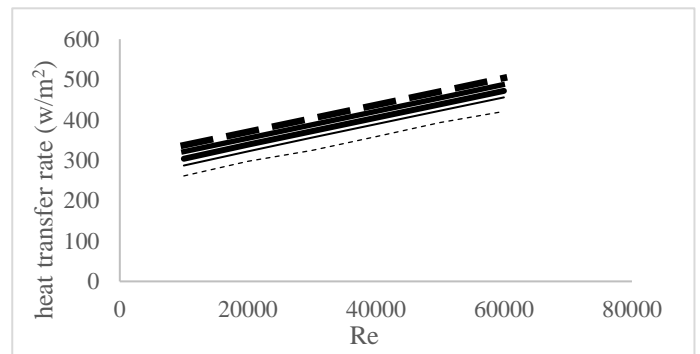
1.Heat Transfer Rate:

Fig.8 Heat Transfer Rate by Computational Analysis

The heat transfer rate of the system can be defined as the amount of thermal energy transfer per unit time (Watt) the above figure explains the plain rib tabulated cooling channel and give less heat transfer rate compared to boot shaped ribs with various Reynolds number ranges from 10000 to 60000. Heat transfer rate can be increased at the place of 3-4 % of incremental in the plain chamber to 3mm, 6mm, 9mm, and 12mm ribbed chambers.
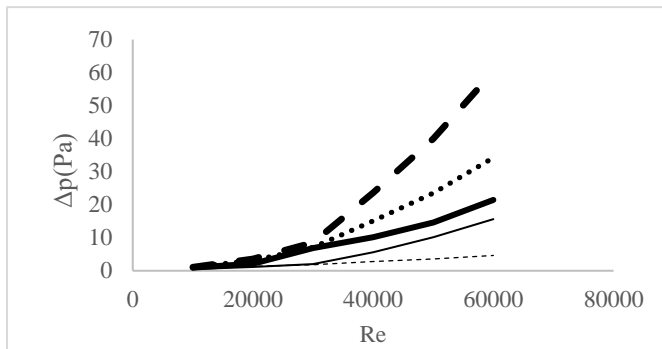
2.Pressure Variation:

Fig.9 Pressure Variation by Computational Analysis

Pressure variations in the rib turbulators with various rib heights based on the Reynolds number variations from 10,000 to 60,000. 12mm rib height can get more pressure change due to the flow separations in 60,000 Reynolds number at the lower Reynolds number the pressure change value is similar to all height of the ribs. It is also observed that If the Reynolds number increases then pressure variation also increases in all geometries. Pressure variation for various ribs has been shown computationally validated.

3.Temperature Variation:

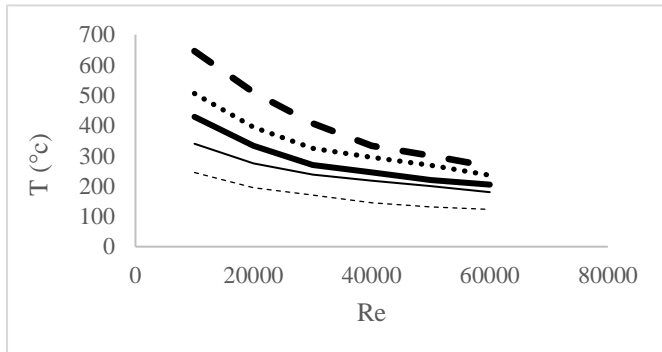

Fig.10 Temperature variation by computational analysis
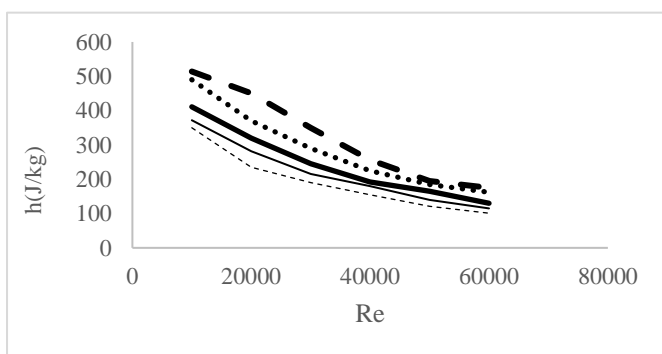
4.Enthalpy(h) Variation

Fig.11 Enthalpy variation by computational analysis

The enthalpy values for different ribs have been obtained using commercial software. The enthalpy value has been measured for different Reynolds number of different ribs of heights as 3mm, 6mm, 9mm, and 12mm. It is found that the enthalpy value is maximum at the lower Reynolds number for 12mm height rib which results in maximum energy released in the thermal system. Enthalpy variation for various ribs from computationally validated.
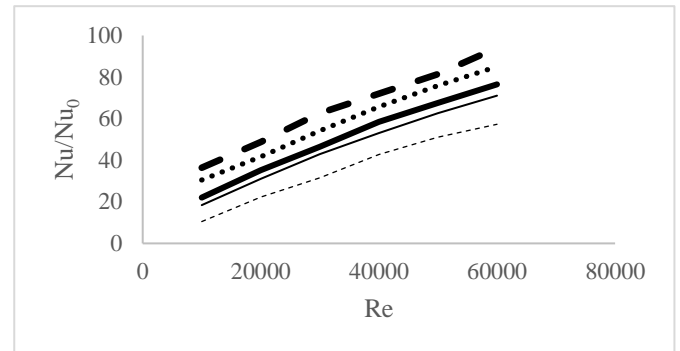
5. Nusselt Number (Nu) Variation:

Fig.12 Nusselt Number variation by computational analysis

The variation of the Nusselt number with increase in the Reynolds number has been shown in the above figure. It is observed that the plain chamber encounter more Nusselt number variations compared to the rib inserted chamber. Nusselt number variation for various ribs from computationally validated.
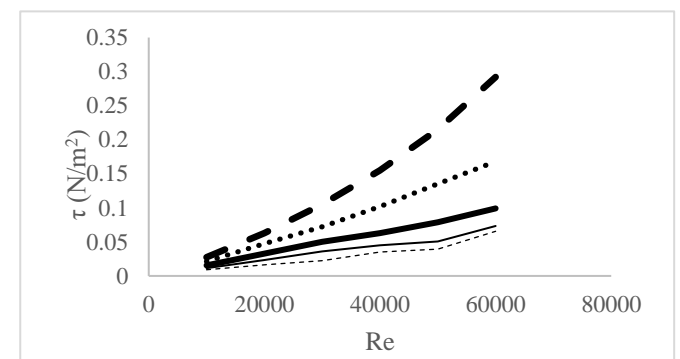
6.Wall Shear Stress(τ) Variation:

Fig.13 Wall Shear Stress by computational analysis

Comparisons of the wall shear stress is a very important factor in the analysis of ribs. Its variation has been predicted with various Reynolds number with the range of 10,000 to 60,000 for different ribs. It's observed from the comparison graph that 12mm ribs have the more wall shear stress and for 6 mm ribs it is lower. Wall shear stress variation for various ribs from computationally validated.

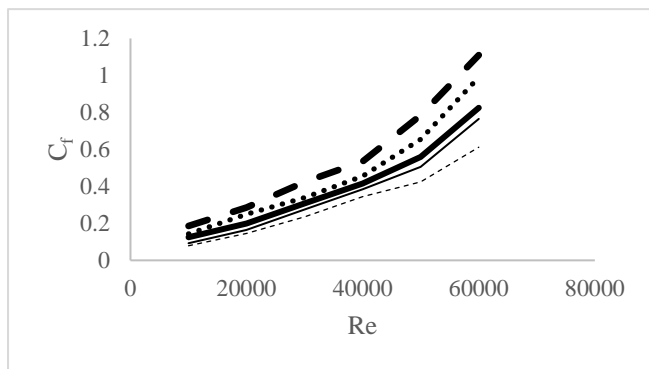## 7.Skin Friction Coefficient (C_f) Variation:

Fig.14 Skin Friction Coefficient by computational analysis

Comparisons of the skin friction coefficient with the various Reynolds number with a various height of the ribs in this comparison chart is shown in the figure. It's observed that 3mm height of the ribs can get the low skin friction factor and 6 mm height of the rib achieved a slightly higher value of skin friction coefficient at higher Reynolds number. It's also observed that 12mm height of the rib gets the maximum skin friction coefficient values. Skin friction coefficient variation for various ribs from computationally validated.

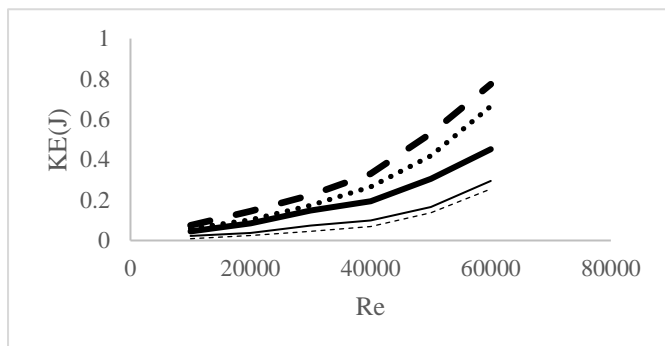## 8.Turbulence Kinetic Energy(K) Variation:

Fig.15 Turbulence Kinetic Energy by computational analysis

From the above chart, it's obvious that the effect of turbulence is higher for ribs with more height and also at higher Reynolds number because of the circulation created at the region behind each rib. Turbulence kinetic energy variation for various ribs from computationally validated.

5.Conclusion

The heat transfer rate of boot-shaped rib has been calculated by providing the various height of the rib from 3-12mm as four various heights with the difference of 3 each. CFD is used to analyse the heat transfer rate of the ribs with respect to Reynolds number for the above-mentioned heights, followed by the pressure variation, temperature variation, enthalpy variation, Nusselt number variation, wall shear stress variation, skin friction coefficient variation and turbulent kinetic energy variation has been calculated with respect to Reynolds number for every different height of rib.

As the flow passes over the rib, the flow separation happens due to adverse pressure gradient which leads to the formation of turbulence behind the ribs. The turbulence in turn increases the heat transfer as its evident by the results.

6.References

[1].Mi-Ae Moon, Min-Jung Park, Kwang-Yong Kim "Evaluation of heat transfer performances of various rib shapes, International Journal of Heat and Mass Transfer" 71 (2014) 275–284.

[2]. Michael Huh, Yao-Hsein Liu, Je-Chin Han "Effect of rib height on heat transfer in a two-pass rectangular channel (AR = 1:4) with a sharp entrance at high rotation numbers, "International Journal of Heat and Mass Transfer" 52 (2009) 4635–4649

[3]. Giovanni Tanda "Effect of rib spacing on heat transfer and friction in a rectangular channel with 45^0 angled rib turbulators on one/two walls, International Journal of Heat and Mass Transfer " 54 (2011) 1081–1090

[4]. Feng Zhang, Xinjun Wang, Jun Li "Effects of coolants on the flow and heat transfer characteristics in a non-rotating and rotating two-pass rectangular channel, International Journal of Heat and Mass Transfer" 91 (2015) 390–400.

[5]. Wei Wang, "Efficiency study of a gas turbine guide vane with a newly designed combined cooling structure, International Journal of Heat and Mass Transfer" 80 (2015) 217–226.

[6]. Prashant Singh, Weihong Li, Srinath V. Ekkad, Jing Ren "Experimental and numerical investigation of heat transfer inside two-pass rib roughened duct (AR = 1:2) under rotating and stationary condition, "International Journal of Heat and Mass Transfer" 113 (2017) 384–398

[7]. Zhongyang Shen, Yonghui Xie, Di Zhang, "Experimental and numerical study on heat transfer in trailing edge cooling passages with dimples/protrusions under the effect of sidewall slot ejection, International Journal of Heat and Mass Transfer" 92 (2016) 1218–1235

[8]. Santosh B. Bopche, Madhukar S. Tandale. "Experimental investigations on heat transfer and frictional characteristics of a turbulator roughened solar air heater duct, International Journal of Heat and Mass Transfer" 52 (2009) 2834–2848

[9]. Gongnan Xie, Jian Liu, Phillip M. Ligrani, BengtSunden"Flow structure and heat transfer in a square passage with offset mid-truncated ribs, "International Journal of Heat and Mass Transfer" 71 (2014) 44–56

[10]. Yu Rao, Christoph Biegger, Bernhard Weigand, "Heat transfer and pressure loss in swirl tubes with one and multiple

tangential jets pertinent to gas turbine internal cooling, "International Journal of Heat and Mass Transfer" 106 (2017) 1356–1367

[11]. Gongnan Xie, Jian Liu, Phillip M. Ligrani, Weihong Zhang, "Numerical analysis of flow structure and heat transfer characteristics in square channels with different internal-protruded dimple geometrics, "International Journal of Heat and Mass Transfer" 67 (2013) 81–97.

[12]. Pey-Shey Wua, Shyy Woei Chang, Chuan-Sheng Chen, Chien-Chou Weng, Yu-Ru Jiang, Shih Hao Shih, "Numerical flow and experimental heat transfer of S-shaped two-pass square channel with cooling applications to gas turbine blade, "International Journal of Heat and Mass Transfer" 108 (2017) 362–373.

[13]. Gongnan Xie, Bengt Sundén, "Numerical predictions of augmented heat transfer of an internal blade tip-wall by hemispherical dimples, International Journal of Heat and Mass Transfer" 53 (2010) 5639–5650

[14]. Huitao Yang, Hamn-Ching Chen, Je-Chin Han, Hee-Koo Moonb, "Numerical study of film cooled rotor leading edge with tip clearance in 1-1/2 turbine stage, International Journal of Heat and Mass Transfer" 51 (2008) 3066–3081

[15]. Hongwu Deng, Yang Li, Zhi Tao, GuoqiangXu, Shuqing Tian, "Pressure drop and heat transfer performance in a rotating two-pass channel with staggered 45-deg ribs, International Journal of Heat and Mass Transfer" 108 (2017) 2273–2282.

[16]. Mi-Ae Moon, Kwang-Yong Kim, "Analysis and optimization of fan-shaped pin–fin in a rectangular cooling channel, International Journal of Heat and Mass Transfer" 72 (2014) 148–162. [17]. Heeyoon Chung, Jun Su Park, Sehjin Park, Seok Min Choi, Dong-Ho Rhee, HyungHee Cho, "Augmented heat transfer with intersecting rib in rectangular channels having different aspect ratios, International Journal of Heat and Mass Transfer" 88 (2015) 357–367

[18]. R. Kan, L. Guo, J. Ren, S. Huang, H.D. Jiang, Y.Y. Yan, "Determining mainstream reference temperature using the non-dimensional temperature analysis in the transient liquid crystal technique, "International Journal of Heat and Mass Transfer" 72 (2014) 201–209

[19]. Zhongyang Shen, Huancheng Qu, Di Zhang, Yonghui Xie, "Effect of bleed hole on flow and heat transfer performance of U-shaped channel with dimple structure, International Journal of Heat and Mass Transfer" 66 (2013) 10–22
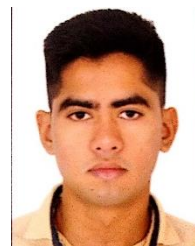
BIOGRAPHIES

Kyada Hiten have completed bachelor degree in aeronautical engineering from K.C.G. College of technology (Anna University), Chennai – 600097, Tamilnadu, India.

Lakkad Harsh have completed bachelor degree in aeronautical engineering from K.C.G. College of technology (Anna University), Chennai – 600097, Tamilnadu, India.

Dave Rutvik have completed bachelor degree in mechanical engineering from S.S.A.S. Institute of Technology(GTU), Surat, Gujarat, India.

Asmaniwala Harsh have completed bachelor degree in mechanical engineering from S.S.A.S. Institute of Technology(GTU), Surat, Gujarat, India.